*This is the peer reviewed version of the following article: Chem. Eur. J. **2017**, 23, 17954-17963, which has been published in final form at https://doi.org/10.1002/chem.201703423. This article may be used for non-commercial purposes in accordance with Wiley Terms and Conditions for Use of Self-Archived Versions.*

Molecular engineering of Mn(II) diamine diketonate precursors for the vapor deposition of manganese oxide nanostructures

Chiara Maccato,[a] Lorenzo Bigiani,[a] Giorgio Carraro,[a] Alberto Gasparotto,[a] Roberta Seraglia,[b] Jiyeon Kim,[c] Anjana Devi,[c] Gloria Tabacchi,*[d] Ettore Fois,[d] Giuseppe Pace,[b] Vito Di Noto,[e] and Davide Barreca*[b]

Abstract: Molecular engineering of Mn(II) diamine diketonate compounds is a key step for their optimization as precursors for the vapor deposition of manganese oxide materials with a variety of technological applications. In the present work, two closely related adducts of Mn(II) of general formula MnL_2•TMEDA [L = 1,1,1,5,5,5-hexafluoro-2,4-pentanedionate (hfa), or 1,1,1-trifluoro-2,4-pentanedionate (tfa); TMEDA = *N*,*N*,*N'*,*N'*-tetramethylethylenediamine] were synthesized by a simple procedure and, for the first time, characterized in detail by a joint experimental-theoretical approach. The main aim was to elucidate their structure, electronic properties, thermal behavior and fragmentation patterns, in order to address the general issue of ligand influence on precursor properties, reactivity and deposition behavior. The obtained compounds are monomeric and characterized by a *pseudo*-octahedral coordination at the Mn(II) center, with fine differences in their structure and fragmentation processes related to the ligand nature. Both compounds can be readily vaporized without premature side decompositions, a favorable feature for their use as precursors for chemical vapor deposition (CVD) or atomic layer deposition (ALD) applications. Preliminary validation experiments evidenced in fact the possibility of obtaining high purity and single-phase Mn_3O_4 nanosystems with tailored morphology on different substrates already at moderate temperatures.

[a] *Prof. C. Maccato, Dr. L. Bigiani, Dr. G. Carraro, Prof. A. Gasparotto, Department of Chemistry, Padova University and INSTM 35131 Padova, Italy*

[b] *Dr. R. Seraglia, Dr. G. Pace, Dr. D. Barreca CNR-ICMATE and INSTM, Department of Chemistry, Padova University 35131 Padova, Italy E-mail: davide.barreca@unipd.it*

[c] *Dr. J. Kim, Prof. A. Devi Inorganic Materials Chemistry, Faculty of Chemistry and Biochemistry, Ruhr-University Bochum 44801 Bochum, Germany*

[d] *Prof. G. Tabacchi, Prof. E. Fois Department of Science and High Technology University of Insubria and INSTM 22100 Como, Italy E-mail: gloria.tabacchi@uninsubria.it*

[e] *Prof. V. Di Noto Department of Industrial Engineering, Chemical Technology Section, in Department of Chemistry, Padova University and INSTM 35131 Padova (PD), Italy*

Supporting information for this article is available on the www under http://dx.doi.org/10.1002/chem. It contains experimental crystallographic data and calculated parameters for MnL_2•TMEDA (Tables S1-S2), NBO charges and bond orders (Tables S3-S4), calculated structures of Mn-containing fragments (Figure S1), components of the π–π* ligand-to-ligand transitions calculated for MnL_2•TMEDA (Figures S2-S3), molecular orbitals involved in the π–π* electronic transitions calculated for the isolated hfa and tfa ligands (Figure S4), MnL_2•TMEDA bond distances, stabilization energies and dipole moments in the presence of an electric field (Table S5), MS^2 and MS^3 mass spectra of selected ions (Figures S5-S7), calculated structures of $[Mn(hfa)_3]^-$ and $[Mn(tfa)_3]^-$ ions (Figure S8).

Introduction

Manganese oxide nanomaterials are of considerable importance in many technological applications, thanks to their structural flexibility endowed with a variety of appealing chemical and physical properties.[1] In particular, Mn_3O_4, a mixed valence state oxide with a tetragonal structure, has received attention thanks to its high activity, durability, and low cost for a variety of end-uses, spanning from (photo)catalysts for various processes,[1a,b,2] to energy-storage materials for anodes of Li-ion batteries and pseudocapacitors,[1b,2b,3] up to electrochromic systems,[4] magnetic media,[5] and gas sensors.[1d,6] In this widespread context, the fabrication of Mn_3O_4 nanostructures with tailored morphology (nanoparticles, nanorods, nanofractals,….) has been carried out through a multitude of synthetic techniques, encompassing microwave irradiation, hydrothermal/solvothermal routes, chemical bath deposition, and chemical vapor deposition (CVD).[1a,b,2a,2c,4-7] In particular, the latter processes, along with atomic layer deposition (ALD), are compatible with current processing standards, thanks to the capacity of achieving *in-situ*, large area and conformal growth on different kinds of substrates. Indeed, CVD and ALD stand as preferred routes to thin films and nanostructured materials with controlled properties,[8] which can be tailored through a proper choice of process conditions and molecular precursors.[9] In particular, the design and development of suitable precursor compounds endowed with high volatility, thermal stability and clean decomposition pathways is a very challenging research area,[10] which would ideally guide, in a 'molecular engineering' approach, the modulation of material properties in view of their ultimate functional applications.

The most used Mn precursors reported so far for CVD and ALD techniques are mainly based on β-diketonate derivatives,[1e,11] some of which suffer from poor shelf life and/or unfavorable thermal properties,[9a] especially if containing Mn(II). In fact, Mn(II) complexes bearing unfluorinated β-diketonate ligands are reported to readily decompose into Mn(III) derivatives,[11d,12] yielding a poor control of the deposition process and phase composition of the resulting products. As a consequence, the obtainment of single-phase Mn_3O_4 nanomaterials with controlled crystallinity and

morphology[13] requires the tailoring of β-diketonate compound properties at a molecular level. In this regard, the use of fluorinated ligands helps in achieving complexes with improved shelf-life, thermal and mass transport properties if compared to conventional compounds.[9a] These features can be synergistically joined with the advantages offered by bidentate diamine ligands to achieve a completely saturated metal coordination sphere - such as in the series of β-diketonate-diamine compounds with general formula M(hfa)$_2$•TMEDA (hfa = 1,1,1,5,5,5-hexafluoro-2,4-pentanedionate). The hfa ligand bears two $-CF_3$ groups, which enhance volatility through the decrease of Van der Waals intermolecular forces[11d] and result in an enhanced Lewis acidity of the metal center,[9a] enabling the stabilization of diamine-containing adducts. Although M(hfa)$_2$•TMEDA complexes of various metal elements present a common structural motif – a *pseudo*-octahedral MO_4N_2 geometry – investigations on Cu,[14] Co,[15] Fe[16] and Zn[17] homologues highlighted that their chemico-physical properties, as well as the features of their CVD products, dramatically depend on the nature of the metal center.

As regards manganese, stable Mn(II) compounds may be obtained by using fluorinated diketonate ligands, such as the widely adopted hfa.[9a,12,18] Now, the question arises as to whether the presence of only one $-CF_3$ group for each diketonate could be sufficient to endow the diamine adducts with the stability, volatility, and clean decomposition properties required for their effective CVD/ALD applications. If the weakest bonds in the complexes, and the first to be broken, certainly depend on the metal center,[14b,16c,17] the effect of the ligands is in fact equally important. Note that a diketonate with a single $-CF_3$ - indicated hereafter as tfa (1,1,1-trifluoro-2,4-pentanedionate) could be formally obtained by replacing one of the hfa fluorinated moieties with a methyl group. How would such a ligand modify the chemistry of these precursors, and to what extent would their performances in CVD processes be affected? Literature, unfortunately, offers no clear answer to these questions. Despite M(tfa)$_2$ complexes have been reported for M = Co,[19] Ni,[20] Cu,[21] M(tfa)$_2$•TMEDA adducts have been much less investigated than their hfa-containing counterparts. In fact, only a work mentioning Cu(tfa)$_2$•TMEDA[22] is available in the literature and no direct connections between the ligand molecular properties and the precursor deposition behavior have been investigated in detail so far.

To elucidate such interrelations, and to address the general issue of the ligand influence on precursor reactivity, we investigate herein the structure/property interplay for two Mn(II) complexes bearing either hexafluorinated or trifluorinated diketonate ligands, namely Mn(hfa)$_2$•TMEDA and Mn(tfa)$_2$•TMEDA. It is worthwhile noticing that, despite the preparation of Mn(hfa)$_2$•TMEDA has already been reported,[23] only some data on its structure and thermal behavior are available in the literature,[12,18] whereas a detailed theoretical-experimental characterization for this compound is completely missing. The need of these studies is even stronger for Mn(tfa)$_2$•TMEDA, which, so far, has been mentioned only once in a patent as antiknock additive.[23]

In this work, our main aim is to disclose how the degree of fluorination of the ligand in the above MnL$_2$•TMEDA precursors affects not only the chemico-physical features, but also their stability, volatility and gas-phase fragmentation, with particular emphasis on their performances in the CVD of Mn_3O_4 nanomaterials. Specifically, the experimental data presented herein for the two complexes are validated and integrated by a detailed DFT modeling, aimed at providing a theoretical basis[24] for the interpretation of similarities and differences in their structure, bonding and chemical behavior. Finally, preliminary results concerning the low-pressure CVD validation of both compounds as Mn molecular sources for Mn_3O_4 nanodeposits on different substrates are also reported.

Results and Discussion

Synthesis and characterization of MnL$_2$•TMEDA compounds

In this work, the MnL$_2$•TMEDA adducts were obtained through a procedure different from that reported in the literature for Mn(hfa)$_2$•TMEDA,[18] involving the reaction in aqueous mixtures between Mn(II) chloride and L ligands in the presence of TMEDA (Scheme 1). The process, carried out at room temperature with no need of refluxing, at variance with a previous study,[12] yielded the target adducts, that could be readily manipulated in the presence of air, moisture and light without any detrimental degradation. Beside a shelf-life of various months, the present MnL$_2$•TMEDA compounds possessed an appreciable volatility (m.p. = 86 and 99°C for L = hfa and tfa, respectively[23]) and could be readily sublimed under vacuum (≈10^{-3} mbar). The melting point of Mn(hfa)$_2$•TMEDA at atmospheric pressure resulted higher than that previously obtained by some investigators,[12,18] but in line with that reported in a patent quoting the use of this compound as a gasoline additive.[23]

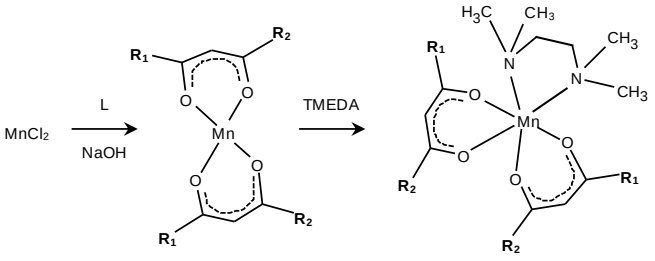

R$_1$ = **R$_2$** = CF_3 ⇒ Mn(hfa)$_2$•TMEDA
R$_1$ = CF_3, **R$_2$** = CH_3 ⇒ Mn(tfa)$_2$•TMEDA

Scheme 1. The synthesis of MnL$_2$•TMEDA derivatives.

The molecular structures of the two complexes are displayed in Figure 1, whereas crystallographic and structural refinement data, as well as geometrical parameters of the DFT-calculated structures, are presented in Tables S1 and S2 in the Supporting Information. Selected bond lengths and angles are listed in Table 1. At variance with other cases, such as that of Mn bis(*N*,*N*'-diisopropylacetamidinate)[25] or variously substituted dialkylmanganese(II) complexes,[8d] both compounds resulted to be monomeric both in the solid state and in solution (see also below for Electrospray Ionization-Mass Spectrometry (ESI-MS) results), indicating that the use of TMEDA was effective in saturating the Mn(II) coordination sphere. In addition, despite the synthesis was carried out in aqueous mixtures, no water molecules were present in the Mn(II) environment, and no classi-

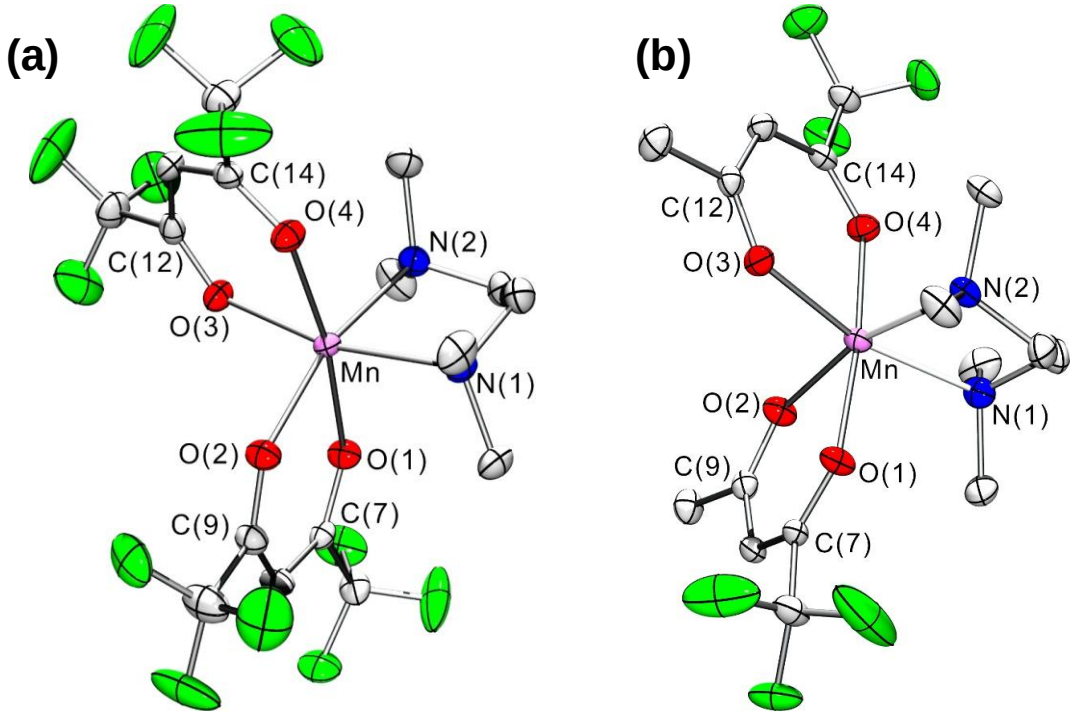

Figure 1. Molecular structures of (a) $Mn(hfa)_2$•TMEDA and (b) $Mn(tfa)_2$•TMEDA. Displacement ellipsoids are shown at the 50% probability level, and hydrogen atoms and rotational disorder from $-CF_3$ group are omitted for clarity.

cal hydrogen bonds were present in the solid state structure. This latter feature is of great importance in view of CVD/ALD utilization[14c,15-16] (see also below for thermoanalytical data). In a different way, for $Mn(hfa)_2$•$2H_2O$[11d] and for other Mn(II) β-diketonates like the adducts of $Mn(hfa)_2$ with substituted nitronyl nitroxides,[26] the occurrence of hydrogen bonding has been reported.

In both cases of Figure 1, X-ray crystal structure determination provided evidence for a *cis* geometry,[27] as also reported for $M(hfa)_2$•TMEDA with M = Fe,[16a] Co[15] and Cu,[14c] with a two-fold axis bisecting the TMEDA ligand. Irrespective of the used β-diketonate, the mean Mn–O and Mn–N bond lengths were in line with those reported in the literature for coordination complexes of 2-(4-quinolyl)nitronyl nitroxide[28] and 2,2'-bipyridine[29] with $Mn(hfa)_2$ and for various Mn(II)-hfa compounds,[9a,11d,18,27] including $Mn(hfa)_2$•TMEDA, though the present work contains a better quality of structure refinement for the latter complex. As can be inferred from Figure 1, a six-fold coordination around Mn(II) centers was evidenced in both cases, resulting in a MnO_4N_2 distorted octahedral environment, in line with previous reports for homologous complexes available in the Cambridge Structural Database.[27] In comparison to other ML_2•TMEDA adducts (M = Fe,[16a] Co,[15] Cu,[14c] Zn[30]), the O–M–O, O–M–N, and N–M–N bond angles (Table 1) are slightly lower (up to ≈5°), whereas M–O and M–N distances are slightly longer. Similarly to the case of the Fe homologue,[16a] the O–C bond lengths of β-diketonate ligands were all close to 1.25 Å, a value suggesting a double bond character (typical O–C single bonds ≈ 1.40 Å). For $Mn(tfa)_2$•TMEDA, atomic distances between O(1)–C(7) and present MnL_2•TMEDA compounds, the Mn–O bonds *trans* to the

Bond lengths (Å)	$Mn(hfa)_2$•TMEDA	$Mn(tfa)_2$•TMEDA
Mn–O(1)	2.1472(14)	2.1481(14)
Mn–O(2)	2.1743(14)	2.1629(14)
Mn–O(3)	2.1546(14)	2.1525(14)
Mn–O(4)	2.1493(14)	2.1265(14)
Mn–N(1)	2.2984(17)	2.3428(18)
Mn–N(2)	2.2989(17)	2.3116(17)
O(1)–C(7)	1.251(2)	1.261(2)
O(2)–C(9)	1.245(2)	1.255(2)
O(3)–C(12)	1.244(3)	1.252(2)
O(4)–C(14)	1.248(3)	1.260(2)
Bond angles (°)		
O(1)–Mn–O(2)	82.07(5)	83.21(6)
O(3)–Mn–O(4)	82.60(5)	83.52(6)
N(1)–Mn–N(2)	79.81(6)	78.66(6)
O(1)-Mn-O(4)	171.03(5)	173.85(6)
O(3)-Mn-N(1)	167.48(5)	166.57(6)
O(2)-Mn-N(2)	166.34(6)	166.49(6)
Mn–O(1)–C(7)	130.02(13)	127.70(13)
Mn–O(2)–C(9)	129.06(13)	130.70(13)
Mn–O(3)–C(12)	128.78(13)	131.12(13)
Mn–O(4)–C(14)	129.13(13)	127.72(13)

Table 1. Selected bond lengths and angles for $Mn(hfa)_2$•TMEDA and $Mn(tfa)_2$•TMEDA.

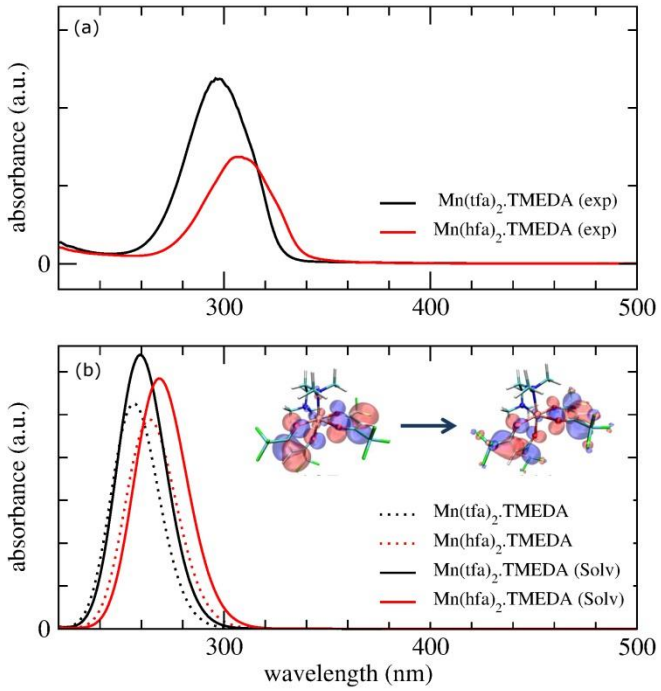

Figure 2. Experimental (a) and theoretical (b) UV-Vis optical spectra for $Mn(hfa)_2$•TMEDA (red lines) and $Mn(tfa)_2$•TMEDA (black lines). The orbitals involved in one of the components of the transition for $Mn(hfa)_2$•TMEDA are shown in the inset of (b) (see Figures S2-S3 in the Supporting Information for graphical representations of all the components for the two complexes). Theoretical spectra were calculated both in vacuum (no label) and with a polarizable continuum model[31] for the solvent ethanol (label 'Solv').

O(4)–C(14) are slightly longer than those of O(2)–C(9) and O(3)–C(12), due to the CF_3– electron withdrawing groups directly bonded to C(7) and C(14) atoms. In addition, for each of the N atoms of the diamine ligand [Mn–O(2) and Mn–O(3)] were slightly longer than those *trans* to the O atoms of L ligands [Mn-O(1) and Mn-O(4); compare the pertaining values, Table 1[9a]].

A similar *trans* effect has already been observed for $M(hfa)_2$•TMEDA compounds with M = Mg,[32] Fe,[16a] Co,[15] Zn.[17,30] Finally, it is worth noting that, for both complexes, Mn–N bonds were longer than Mn–O ones. This effect, which was particularly evident for $Mn(tfa)_2$•TMEDA, anticipated an easier opening of the TMEDA ring with respect to the β-diketonate one, as indeed suggested by the calculated bond orders, electronic population analyses and decomposition energies for the two precursors. In both complexes – particularly in the case of $Mn(tfa)_2$•TMEDA - the diketonate is a stronger electron donor towards Mn if compared to the diamine (Table S3 in the Supporting Information). Accordingly, Mn–N bonds are significantly weaker than Mn–O ones (Table S4 in the Supporting Information), suggesting that, at least in the gas phase, the TMEDA ligand should be more easily released compared to the diketonate one. On this basis, we calculated the decomposition energy of the complexes ΔE for the following pathways (equations (1) and (2), with L=hfa/tfa) in vacuum and in methanol, *i.e.* the solvent used in the present ESI-MS experiments:

$$Mn(L)_2\text{•TMEDA} \rightarrow MnL\text{•TMEDA}^+ + L^- \quad (1)$$

$$Mn(L)_2\text{•TMEDA} \rightarrow MnL_2 + TMEDA \quad (2)$$

As a first step, the geometries of $MnL\text{•TMEDA}^+$ and MnL_2 fragments were optimized in vacuum. The loss of one ligand strongly desaturates the Mn coordination sphere: all fragments exhibit a tetrahedral coordination, as depicted in Figure S1 in the Supporting Information. For L = hfa, calculations yielded ΔE_1 = 125.4 kcal×mol^{-1} and ΔE_2 = 38.0 kcal×mol^{-1}, whereas the corresponding values for L = tfa were ΔE_1 = 131.3 kcal×mol^{-1} and ΔE_2 = 31.0 kcal×mol^{-1}. Hence, in the gas phase, the loss of a hfa/tfa moiety would be severely unfavored against the loss of TMEDA, in line with the previously discussed data. Nevertheless, when the same quantities are calculated in methanol,[31] the difference decreases substantially, indicating that the energetic costs of the two decomposition routes become comparable. This is particularly evident for L = hfa, where ΔE_1 = 30.3 kcal×mol^{-1} and ΔE_2 = 28.8 kcal×mol^{-1}, while for L = tfa we found ΔE_1 = 32.9 kcal×mol^{-1} and ΔE_2 = 23.3 kcal×mol^{-1}. The reaction medium plays therefore a key influence on fragmentation pathways. Fragmentation route (1), highly unfavored in vacuum, becomes viable in a polar solvent due to the stabilization of the resulting ionic species. This might be particularly important for ESI-MS experiments, where the first fragmentation of the complex normally occurs in the solvent medium, as discussed in the following. On the other hand, route (2) should be favored in the gas-phase, such as in thermal CVD experiments.

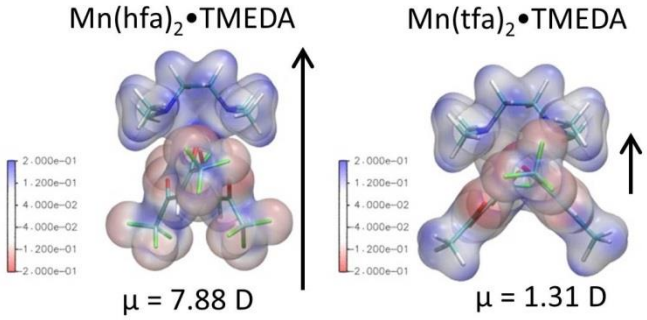

Figure 3. Electrostatic potential map for $Mn(hfa)_2$•TMEDA and $Mn(tfa)_2$•TMEDA. Regions of high (positive) potential (in blue) are electron-poor, whereas regions of low (negative) potential (in red) are electron-rich. White/grey colors represent intermediate electrostatic potential values. Arrows indicate the direction and magnitude of the electric dipole moments μ. Atom color codes: Mn = pink; F = green; O = red; N = blue; C = cyano; H = white.

Focusing on the electronic properties of the two complexes, the broad band at λ≈300 nm in the UV-Vis spectra (Figure 2) is due to electronic states mostly localized on the diketonate ligands (see inset in Figure 2b). More specifically, the electronic transition arises from π– π* ligand-to-ligand excitations (see Figures S2-S4 in the Supporting Information). The calculated spectra reproduce the obtained experimental trend, with a spectral shift to higher wavelenghts for $Mn(hfa)_2$•TMEDA compared to $Mn(tfa)_2$•TMEDA, and the agreement is further improved if the solvent contribution is taken into account. The same trend is found for the π–π* transitions in isolated hfa and tfa (see Figure S4 in the Supporting Information), indicating that the electronic excitation and optical properties of the complexes are dominated by the ligand nature.

This finding prompted us to investigate more closely the ligand effect on the electronic structure and the electric dipole moment of the complexes. Results showed that $Mn(hfa)_2$•TMEDA has a dipole moment considerably larger than $Mn(tfa)_2$•TMEDA, due to the net charge separation between hfa and diamine ligands, as depicted in the electrostatic potential maps (Figure 3). Indeed, whereas the electrostatic potential of TMEDA is positive, and that of hfa is negative, the tfa ligand exhibits both positive and negative regions, localized on the $–CH_3$ and $–CF_3$ groups, respectively. The application of external electric fields, as in ESI-MS experiments (see below), might thus have different effects on the two

compounds. Calculations indicated that both complexes were slightly stabilized by a moderate electric field and showed a small increase of the dipole moment, especially $Mn(hfa)_2$•TMEDA (see Table S5 in the Supporting Information). Such an electric field, therefore, would favor a preferential orientation of the complexes, with an enhanced effect for $Mn(hfa)_2$•TMEDA due to its more asymmetric charge distribution (Figure 3).

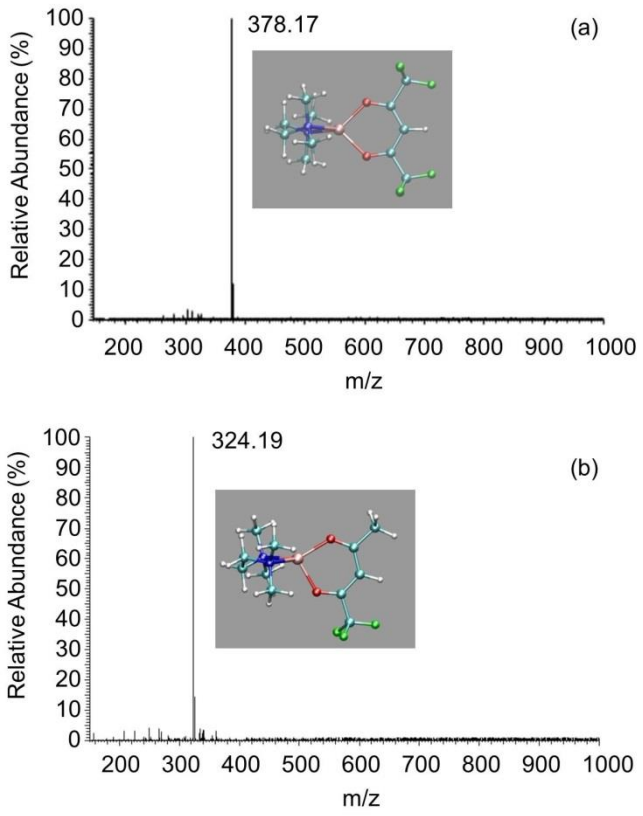

Figure 4. Positive ion ESI-MS spectra of (a) $Mn(hfa)_2$•TMEDA and (b) $Mn(tfa)_2$•TMEDA methanolic solutions. Calculated optimized structures for the most abundant ionic species are shown as insets. Atom color codes as in Figure 3.

An additional insight into the behavior of the two Mn complexes was obtained by means of ESI-MS, a soft ionization technique yielding important information on the compound reactivity. ESI-MS analyses were carried out in both positive (+) and negative (-) ion modes, in order to elucidate the adduct fragmentation pathways and their interrelations with the pertaining molecular structures. It is worthwhile observing that, to the best of our knowledge, no such investigation on MnL_2•TMEDA compounds has ever been reported in the literature up to date.

In positive ion mode, the behavior of the two complexes was qualitatively similar, irrespective of the ligand nature. ESI(+) mass spectra (Figure 4) are in fact dominated by single peaks centered at *m*/*z* 378 and 324, corresponding to $[Mn(hfa)•TMEDA]^+$ and $[Mn(tfa)•TMEDA]^+$, respectively. This result was in agreement with those previously obtained for analogous $M(hfa)_2$•TMEDA compounds, with M = Cu and Co.[14a,14c,15]

To attain a deeper insight into the complex fragmentation pathways, MS^2 and MS^3 experiments were carried out on $[MnL•TMEDA]^+$ ions (see Figures S5-S6 in the Supporting Information). In both cases, irrespective of the ligand nature, MS^2 spectra were characterized by the presence of ions at *m*/*z* 190 and 115 corresponding to diamine-related derivatives, the first of which arose from a ligand-to-metal fluorine transfer process. This behavior was directly dependent on the metal nature, since similar MS^2 experiments on $[M(hfa)•TMEDA]^+$ ions yielded $[CuTMEDA - H]^+$, for the copper derivative,[14a,14c] and $[CoF_2•TMEDA + H]^+$, for the Co one.[15]

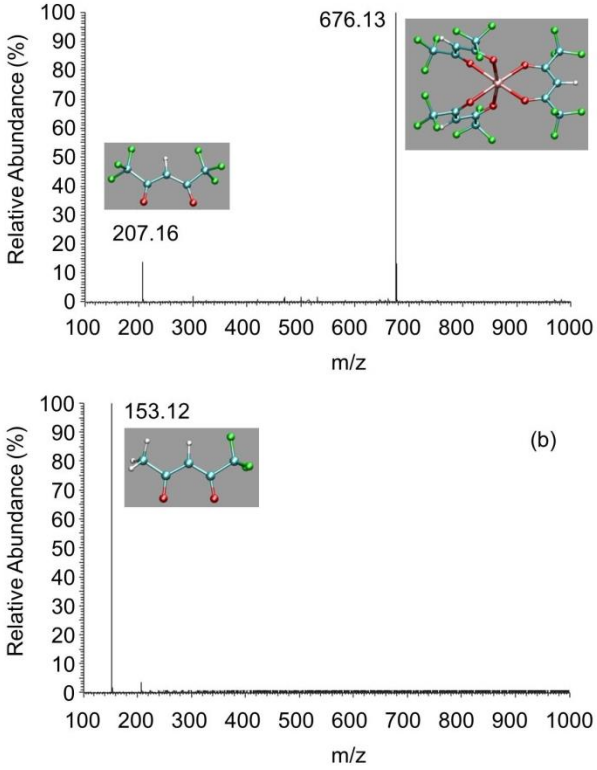

Figure 5. Negative ion ESI-MS spectra of (a) $Mn(hfa)_2$•TMEDA and (b) $Mn(tfa)_2$•TMEDA methanolic solutions. Calculated optimized structures for the most abundant ionic species are shown as insets. Atom color codes as in Figure 3.

In negative ion mode, MnL_2•TMEDA ESI-MS spectra revealed a diverse influence of hfa/tfa ligands on the fragmentation pathway. ESI(-) mass spectrum of $Mn(hfa)_2$•TMEDA (Figure 5a) was characterized by the presence of ions at *m*/*z* 676 and 207, corresponding to $[Mn(hfa)_3]^-$ and $[hfa]^-$, respectively. In a different

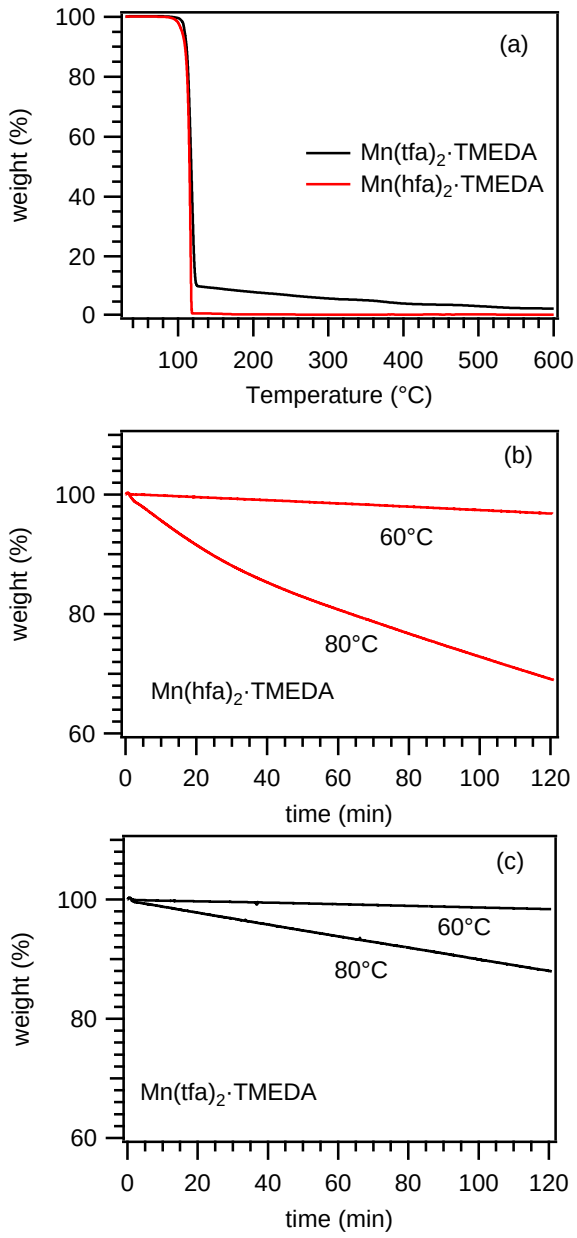

Figure 6. (a) TGA profiles for MnL_2•TMEDA complexes. Isothermal weight changes recorded for: (b) $Mn(hfa)_2$•TMEDA; (c) $Mn(tfa)_2$•TMEDA.

way, the corresponding spectrum of $Mn(tfa)_2$•TMEDA (Figure 5b) evidenced only the signal at *m*/*z* 153, corresponding to $[tfa]^-$ ions. MS/MS experiments on $[Mn(hfa)_3]^-$ ions led to the sole formation of hfa^- (see Figure S7 in the Supporting Information), in accordance with previous results obtained in the ESI-MS analysis of $Fe(hfa)_2$•TMEDA.[16a] The different behavior of the two complexes emerging from Figure 5 suggested a different binding capacity of hfa and tfa ligands towards Mn centers. Indeed, both $[ML_3]^-$ adducts were predicted to be stable with respect to the separated L^- and ML_2 fragments, but the calculated formation energies differ by 2.0 kcal×mol^{-1} in methanol (7.4 kcal×mol^{-1} in vacuum) in favor of $[Mn(hfa)_3]^-$ (see Figure S8 in the Supporting Information). Furthermore, as the formation of $[ML_3]^-$ adducts would involve the fragmentation of at least two ML_2•TMEDA molecules, it might be reasonably argued that the higher dipole moment of $Mn(hfa)_2$•TMEDA could promote a head-to-tail alignment of two such molecules, enhancing the probability of a successful hfa/TMEDA ligand exchange leading to the observed anion. Finally, it is worth noticing that no dimer/polynuclear species have ever been detected. Considering the ESI-MS soft ionization conditions, this result suggests that both complexes are monomeric, in tune with structural analyses (see above).

To be successfully employed as CVD/ALD precursors, the target compounds should possess sufficient stability to ensure transport into the gas phase free from side decomposition, as well as a constant and reproducible vapor supply at a specific temperature. To assess the precursor thermal properties as a function of the ligand nature, thermogravimetric (TGA) analyses were performed for both ML_2•TMEDA compounds, yielding very similar results either for freshly synthesized or for aged sample batches. As can be observed in Figure 6a, both the target adducts displayed a qualitatively similar behavior, characterized by a single-step mass loss for $T \geq 120$°C, indicating a high volatility. As concerns $Mn(hfa)_2$•TMEDA, the residual weight was close to zero for $T \geq 150$°C, evidencing the occurrence of a clean and quantitative vaporization in a narrow temperature range. Such a behavior appears extremely favorable for CVD/ALD applications, especially if compared with commonly adopted Mn precursors, that show either a lower volatility [as observed for $Mn(dpm)_3$, where dpm = 2,2,6,6-tetramethyl-3,5-heptanedionate] or multi-stage decompositions, with a high residual weight [as in the case of $Mn(acac)_2(H_2O)_2$, where acac = 2,4-pentanedionate].[11c,12] Differential scanning calorimetry (DSC) analyses (not reported) enabled to identify the presence of two endothermic peaks at 84.5 and 100.6°C for $Mn(hfa)_2$•TMEDA and $Mn(tfa)_2$•TMEDA, respectively, related to melting processes. In line with melting point values, $Mn(tfa)_2$•TMEDA presented a slightly higher volatilization onset than $Mn(hfa)_2$•TMEDA, a feature that could be attributed to the lower fluorine content of the former compound (see above).[11d] In addition, a non-zero residual weight, progressively lowering for temperatures comprised between 130 and 600°C, could be observed.

Isothermal analyses (Figures 6b-c) carried out for 2 h evidenced a nearly constant weight loss as a function of time for both compounds. Such results, in line with previous reports on Fe, Co and Cu hfa derivatives,[14c,15-16] enabled to rule out significant detrimental decomposition phenomena during vaporization, an issue of critical importance to ensure a constant vapor supply in CVD/ALD applications.

CVD depositions from ML_2•TMEDA

An important point of this study has been the functional validation of ML_2•TMEDA compounds, in order to assess their potential as CVD precursors for the fabrication of manganese oxide nanosystems. Preliminary deposition experiments were carried out on both Si(100) and SiO_2 substrates, using vaporization temperature (≤65°C) and growth temperatures (400°C) lower than those previously adopted in vapor phase processes from $Mn(hfa)_2$, $Mn(hfa)_2$•TMEDA, and $Mn(dpm)_3$.[1e,11a,b,11e,12,18] The obtained brownish samples, characterized by a good adhesion with the substrate, were preliminarily investigated by X-ray diffraction (XRD, Figure 7), which provided evidence for the obtainment of body-centered tetragonal Mn_3O_4 (*haussmannite*; space group

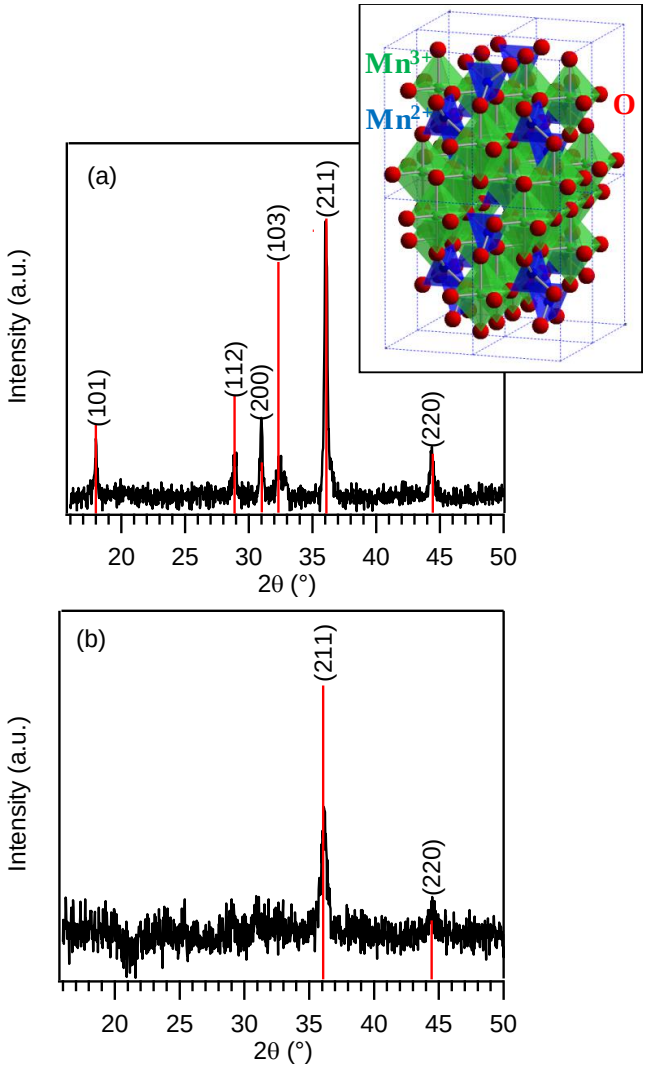

Figure 7. Glancing angle XRD patterns of Mn_3O_4 systems deposited at 400°C: a) on Si(100), from $Mn(hfa)_2$•TMEDA; b) on SiO_2, from $Mn(tfa)_2$•TMEDA. Vertical bars mark the relative intensities of Mn_3O_4 powder spectrum. Inset: representation of the Mn_3O_4 solid state structure.[33]

$I4_1/amd$;[1a,2a,33] lattice parameters a = 5.762 Å, c = 9.470 Å), with Mn(III) and Mn(II) centers in octahedral and tetrahedral sites, respectively[2b,5b,7] (Figure 7, inset). Irrespective of the used substrate, no reflections related to other Mn oxides or Mn(II) fluoride could be detected, indicating the formation of phase-pure systems. The mean crystallite size was (40±5) nm. The system morphology, analyzed by means of field emission-scanning electron microscopy (FE-SEM, Figures 8a-b), revealed the presence of well interconnected lamellar structures [average dimensions = (270±50) nm] uniformly distributed over the substrate surface. The mean nanodeposit thickness was estimated to be (350±20) nm. The measurement of the latter value enabled to estimate an average growth rate of 6 nm×min^{-1}.

The compositional purity of Mn_3O_4 systems was confirmed by energy dispersive X-ray spectroscopy (EDXS) analysis. The obtained spectrum (Figure 8c) showed the presence of MnKα and MnKβ peaks located at 5.90 and 6.50 keV, as well as the OKα signal at 0.52 keV. No evidences of C or F presence could be detected, in agreement with the clean precursor decomposition discussed above. Irrespective of the analyzed region, in-plane EDXS analyses highlighted a homogeneous lateral distribution of oxygen and manganese.

Efforts were also devoted to the chemico-physical characterization of systems supported on silica. To this regard, the surface morphology was investigated by atomic force microscopy (AFM) (Figures 9a-b), that showed the presence of well interconnected protruding nanograins. The deposit appeared homogeneous and free from cracks/pinholes. From the line height profile, a root mean square (RMS) roughness of 5 nm could be estimated.

Finally, optical absorption analyses were also carried out (Figure 9c). The spectral shape was in line with that reported for Mn_3O_4-based materials.[4] As can be observed, the system was almost transparent in the IR range, whereas the significant absorption at lower wavelengths (λ<600 nm) corresponded to interband transitions. The optical band gap was estimated by the Tauc method, plotting $(\alpha h\nu)^n$ *vs.* $h\nu$ (Figure 9c, inset), with n = 2 corresponding to direct allowed transitions,[1d,34] and extrapolating the obtained trend to zero absorption. The estimated energy gap value (E_G = 2.5 eV) was in line with previous literature data for Mn_3O_4,[4-5] and highlighted the efficient harvesting of Vis light, paving the way to the use of the developed materials in solar-assited photoactivated applications.

Conclusions

The present work has been devoted to the preparation and joint experimental/theoretical characterization of two different Mn(II) diamine diketonate adducts, of interest as molecular precursors for the vapor deposition of Mn oxide nanomaterials. The target compounds, $Mn(hfa)_2$•TMEDA and $Mn(tfa)_2$•TMEDA, designed as alternatives to the well known manganese β-diketonates, differ for the presence of one $-CF_3$ group in the ligand chain.

The two compounds, obtained by a simpler route than that previously reported for $Mn(hfa)_2$•TMEDA, are monomeric and water-free, thanks to the complete saturation of Mn(II) coordination environment. In particular, fluorine presence in the diketonate moieties plays a key role towards the stabilization of the complexes and the obtainment of favorable precursor properties (thermal behavior and gas-phase reactivity) for CVD/ALD applications.

The obtained results highlight that variations in the fluorine content of β-diketonate ligands does not affect appreciably the stability to air and moisture of these precursors. The few important differences in the behavior of the two compounds, experimentally highlighted by ESI fragmentation patterns, should mainly be related to the different charge distribution in their molecular structures depending on the nature of β-diketonate ligand. Both compounds exhibit a higher volatility than conventional Mn β-diketonates, paving the way to their successful application for the vapor phase deposition of Mn oxides. Preliminary CVD experiments enabled the preparation of high purity, single-phase Mn_3O_4 nanomaterials endowed with tailored morphology, as well as an appreciable Vis light absorption. The

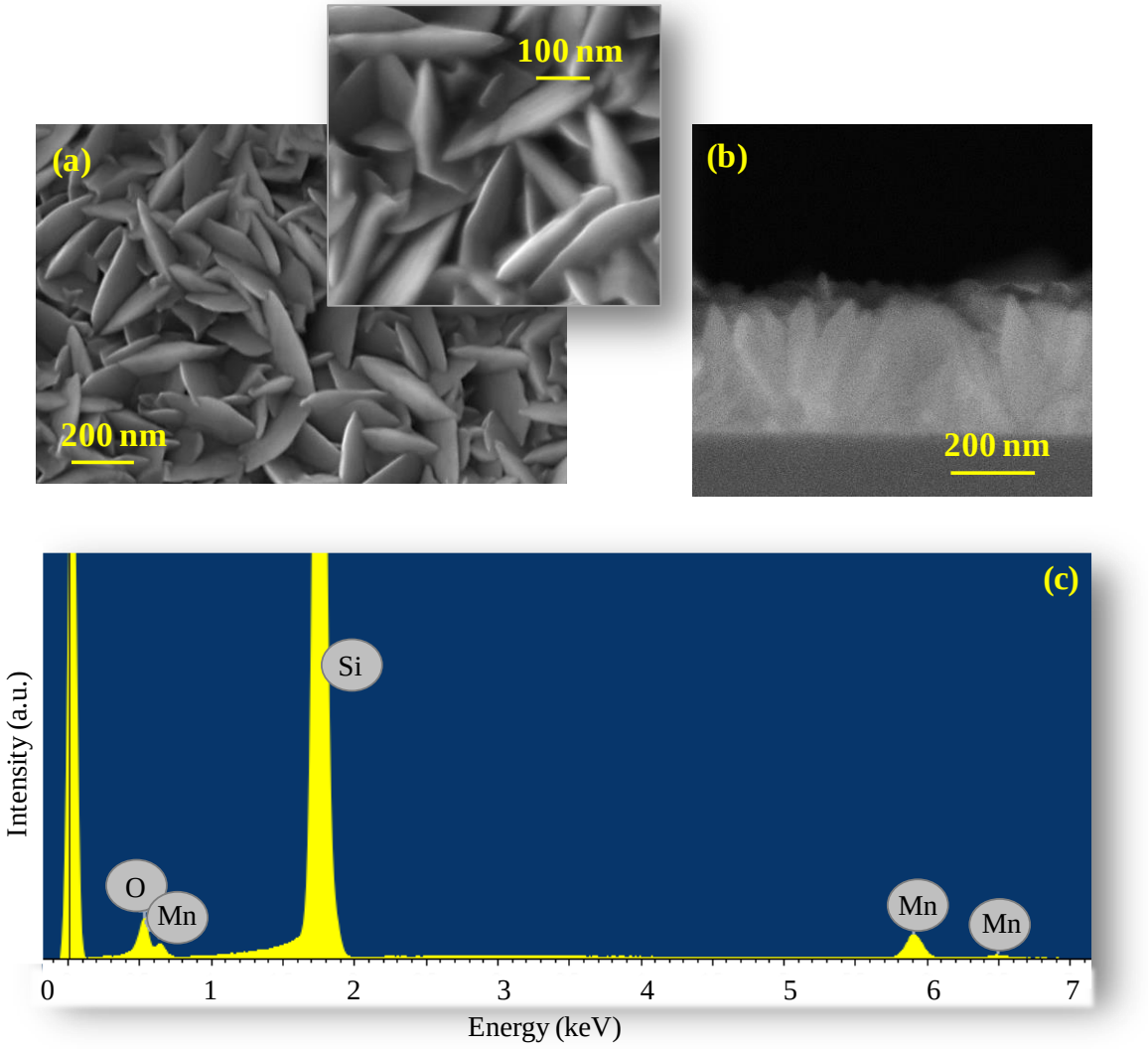

Figure 8. (a) Plane-view and (b) cross-sectional FE-SEM micrographs of a Mn_3O_4 specimen deposited on Si(100) at 400°C from $Mn(hfa)_2$•TMEDA. (c) Corresponding EDXS spectrum.

obtained results candidate the developed nanosystems for possible technological utilization in solar driven processes, ranging from photoactivated H_2O splitting towastewater purification. Additional attractive perspectives for the prosecution of this work will involve the use of both molecular compounds in CVD/ALD processes, to explore in detail the interplay between processing parameters and the resulting material properties. Preliminary studies in this research area are actually being carried out within our group.

Experimental Section

General procedures

$MnCl_2$•$4H_2O$ (98+%), Hhfa (98%) and Htfa (98%) were purchased from Strem Chemicals® and TMEDA (≥98%) from Merck®; all were used without further purification. All manipulations were carried out under normal laboratory conditions. The complex melting points (m.p.) were measured in air by a FALC melting point device at atmospheric pressure. Elemental analyses were carried out by a Fisons Carlo Erba EA1108 apparatus (CHNS version).

Synthesis of $Mn(hfa)_2$•TMEDA

The synthesis of the target adduct was performed following a different procedure with respect to that previously reported.[12,18] To a stirred aqueous solution of $MnCl_2$•$4H_2O$ (2.37 g, 11.73 mmol, in 50 mL of deionized H_2O) were slowly added 3.4 mL of Hhfa (d = 1.47 g×mL^{-1}, 23.30 mmol). The subsequent dropwise addition of NaOH (0.93 g, 23.50 mmol, in 10 mL deionized H_2O) yielded a clear yellow solution. 1.9 mL of TMEDA (d = 0.78 g×mL^{-1}, 12.59 mmol) were then slowly added to the reaction mixture, that turned to a maroon-like color. After reacting for 150 min in the dark, the obtained product was repeatedly extracted in dichloromethane up to the obtainment of a completely colorless aqueous phase. The organic solution was thoroughly washed with deionized water and the solvent was removed at room temperature under reduced pressure (≈10^{-3} mbar), ultimately affording a yellow-orange solid. Yield: 5.15 g (75%); m.p. = 86°C at 1 atm; elemental analysis calcd. (%) for $C_{16}H_{18}O_4N_2F_{12}Mn$ (M_w = 585.25): C 32.84, H 3.10, N 4.79; found: C, 33.60; H, 2.90; N, 4.78.

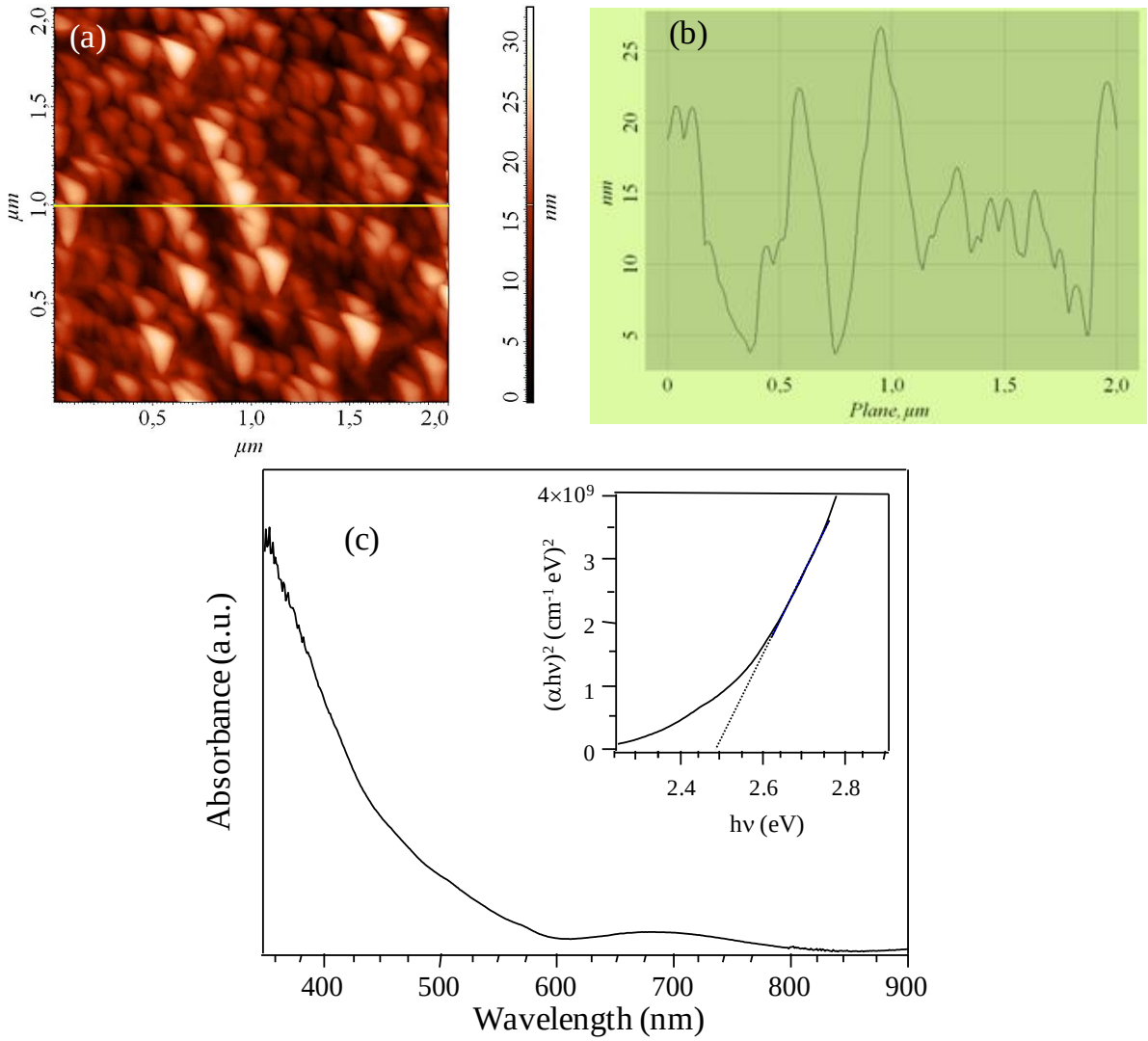

Figure 9. (a). Representative AFM image; (b) height profile along the marked line, and (c) optical spectrum and derived Tauc plot for a Mn_3O_4 deposit obtained on SiO_2 at 400°C from $Mn(tfa)_2$•TMEDA.

Synthesis of $Mn(tfa)_2$•TMEDA

To an aqueous solution of $MnCl_2$•$4H_2O$ (2.37 g, 11.73 mmol, in 50 mL of.deionized H_2O), maintained under vigorous stirring, were slowly added 2.9 mL of Htfa (d = 1.27 g×mL^{-1}, 23.30 mmol), resulting in a phase separation. Subsequently, an NaOH solution (0.93 g, 23.50 mmol, in 10 mL deionized H_2O) was added dropwise, resulting in the formation of a yellow solution. 1.9 mL of TMEDA (d = 0.78 g×mL^{-1}, 12.59 mmol) were then added to the reaction mixture, which became maroon-like. After reaction in the dark for 150 min, the obtained product was repeatedly extracted in dichloromethane until the aqueous phase turned colorless. The organic solution was washed with deionized water and the solvent removed at room temperature (≈10^{-3} mbar), yielding a light yellow solid. Yield: 3.7 g (66%); m.p. = 99°C at 1 atm; elemental analysis calcd (%) for $C_{16}H_{24}O_4N_2F_6Mn$ (M_w = 477.31): C 40.26, H 5.07, N 5.87; found: C, 40.93; H, 5.10; N, 6.03.

Both $Mn(hfa)_2$•TMEDA and $Mn(tfa)_2$•TMEDA were stored at room temperature and could be easily manipulated in air without any detrimental degradation. The powders were soluble in various solvents, such as hexane, dichloromethane, acetone and alcohols. In both cases, crystals for X-ray analysis were obtained by re-dissolution in 1,2-dicholoroethane, followed by slow solvent evaporation.

X-ray crystallography

X-ray diffraction data for the synthesized compounds were collected on an Agilent Technologies SuperNova diffractometer with an Atlas CCD detector, using CuKα radiation (λ = 1.54184 Å) from multilayer X-ray optics. The crystals were coated with a perfluoropolyether, picked up with a glass fiber, and mounted in the nitrogen cold gas stream of the diffractometer. The obtained data were processed with CrysAlisPro.[35] An absorption correction based on multiple-scanned reflections was carried out with ABSPACK in CrysAlisPro. The crystal structure was solved by direct methods using SHELXS-97 and refined with SHELXL-2013.[36] In case of $Mn(hfa)_2$•TMEDA, two of the CF_3 groups showed rotational disorder. Disordered parts were modeled with appropriate restraints and constraints on geometry and atomic displacement parameters (ADPs). Anisotropic ADPs were introduced for all non-hydrogen atoms. Hydrogen atoms were placed in geometrically calculated positions and refined with the appropriate riding model.

Analysis techniques

Optical spectroscopy analyses were carried out using a Cary 50 spectrophotometer (Varian; spectral bandwidth = 1 nm). Measurements were carried out on 10^{-6} M ethanol solutions of both $Mn(hfa)_2$•TMEDA and $Mn(tfa)_2$•TMEDA, using quartz couvettes (optical path = 0.5 cm).

ESI-MS characterization was carried out using a LCQ Fleet ion trap instrument (ThermoFisher), operating in both positive and negative ion modes. The used entrance capillary temperature and voltage were set at 250°C and 4 kV, respectively. 10^{-6} M solutions of the target Mn compounds in methanol were introduced by direct infusion using a syringe pump (flow rate = 8 μL×min^{-1}). MS^n experiments were performed by applying a supplementary Radio Frequency (RF) voltage to the end caps of the ion trap (5 V peak-to-peak).

TGA analyses were performed with a TGA 2950 thermobalance manufactured by TA Instruments. Measurements were conducted under a pre-purified nitrogen atmosphere (heating rate = 10°C×min^{-1}) on samples which had a mass between 5 and 10 mg. DSC analyses were carried out using a MDSC2920 apparatus (TA Instruments) equipped with a liquid nitrogen cooling system using a heating rate of 3°C×min^{-1}.

Simulation

DFT calculations on $Mn(hfa)_2$•TMEDA and $Mn(tfa)_2$•TMEDA were performed with the PBE functional[37] augmented with the long-range corrections of Hirao.[38] Gaussian 09 was adopted,[39] with Stuttgart-Dresden ECP pseudopotential for Mn and Stuttgart-Dresden basis set for all atoms.[40] Such basis set was enhanced with diffuse and polarization functions from the (D95++(d,p)) basis set,[41] which provided a satisfactory description of other members of the $M(hfa)_2$•TMEDA series.[14a,14c,16a,b,17] All calculated minima had positive frequencies and were in the high-spin state (sextet). The spin state was established by optimizing the compounds geometry in the sextet, quartet and doublet state. Electronic excitations were calculated on the minimum energy structures by time-dependent (TD) DFT. The 50 excitations at lower energy were considered. The spectra reported in Figure 2b were obtained by smoothing the TD-DFT excitations with a 2 nm gaussian broadening. TD-DFT excitations were calculated for the two complexes also in ethanol, using a polarizable continuum model for the solvent.[31] Natural Bond Orbitals (NBO) wavefunction analyses were performed with NBO 5.0.[42] Decomposition energies ΔE of the complexes with respect to the fragments keep into account the zero-point-energy contributions and basis-set-superposition errors were counterpoise-corrected. Besides in vacuum, ΔE were calculated in methanol with a polarizable continuum model.[31]

CVD synthesis and characterization of Mn_3O_4 nanomaterials

Manganese oxide depositions were performed by means of a custom-built cold-wall CVD reactor,[16a] using $Mn(hfa)_2$•TMEDA and $Mn(tfa)_2$•TMEDA precursors contained in an external glass reservoir. In this study, the precursor vaporization temperatures were kept at 60°C and 65°C for $Mn(hfa)_2$•TMEDA and $Mn(tfa)_2$•TMEDA, respectively, while the substrate temperature was maintained at 400°C. Gas lines and valves connecting the precursor vessel and the reactor were maintained at T≥100°C for each growth process to prevent precursor condensation. Depositions were carried out in O_2-based atmosphere for 1 h on 1×1 cm^2 Si(100) (MEMC®, Merano, Italy) and Herasil silica (Heraeus®) substrates, which were subjected to suitable pre-cleaning procedures before CVD experiments. For silicon substrates, the native SiO_x layer was removed prior to deposition by means of HF etching. O_2 [total flow rate = 200 standard cubic centimetres per minute (sccm)] was used as carrier and reaction gas. The mass flows were controlled with MKS flow meters (Andover, Usa). The total pressure, measured by a capacitance manometer (BOC Edwards, Crawley, UK) was set at 10.0 mbar.

XRD patterns were recorded in glancing incidence mode (1°) on a Bruker D8 Advance X-ray diffractometer, equipped with a CuKα X-ray source (40 kV, 40 mA) and a Göbel mirror. Crystallite dimensions were estimated by the Scherrer equation.

FE-SEM analyses were performed by a Zeiss SUPRA 40 VP instrument, equipped with an Oxford INCA x-sight X-ray detector for EDXS investigation (primary beam voltage = 20 kV).

Optical absorption spectra for samples deposited on silica substrates were collected in transmission mode at normal incidence by means of a Cary 50 spectrophotometer, subtracting the substrate contribution. Tauc plots based on the obtained data were used to determine the optical band gap.

AFM measurements were performed by a NT-MDT SPM solver P47H-PRO apparatus, operating in tapping mode. RMS roughness values were obtained from the analysis of 2×2 μm^2 images after plane fitting.

Acknowledgements

The authors kindly acknowledge the financial support under Padova University ex-60% 2014–2017, Insubria University FAR 2015-2016, P-DiSC #SENSATIONAL BIRD2016-UNIPD projects and ACTION post-doc fellowship. Thanks are also due to Mr. Loris Calore and to Mr. Filippo Gri (Padova University) for elemental microanalyses and useful experimental assistance.

Keywords: Mn β-diketonates • single-crystal X-ray diffraction • chemical vapor deposition • manganese oxides • nanomaterials

[1] a) Z. Chen, Z. Jiao, D. Pan, Z. Li, M. Wu, C.-H. Shek, C. M. L. Wu, J. K. L. Lai, *Chem. Rev.* **2012**, *112*, 3833-3855; b) Z. Bai, B. Sun, N. Fan, Z. Ju, M. Li, L. Xu, Y. Qian, *Chem. Eur. J.* **2012**, *18*, 5319-5324; c) C. E. Frey, P. Kurz, *Chem. Eur. J.* **2015**, *21*, 14958-14968; d) L. Ben Said, A. Inoubli, B. Bouricha, M. Amlouk, *Spectrochim. Acta, Part A* **2017**, *171*, 487-498; e) O. Nilsen, H. Fjellvåg, A. Kjekshus, *Thin Solid Films* **2003**, *444*, 44-51.

[2] a) Z.-Y. Fei, B. Sun, L. Zhao, W.-J. Ji, C.-T. Au, *Chem. Eur. J.* **2013**, *19*, 6480-6487; b) K. Wang, X. Ma, Z. Zhang, M. Zheng, Z. Geng, Z. Wang, *Chem. Eur. J.* **2013**, *19*, 7084-7089; c) D. M. Robinson, Y. B. Go, M. Mui, G. Gardner, Z. J. Zhang, D. Mastrogiovanni, E. Garfunkel, J. Li, M. Greenblatt, G. C. Dismukes, *J. Am. Chem. Soc.* **2013**, *135*, 3494-3501.

[3] M.-K. Song, S. Cheng, H. Chen, W. Qin, K.-W. Nam, S. Xu, X.-Q. Yang, A. Bongiorno, J. Lee, J. Bai, T. A. Tyson, J. Cho, M. Liu, *Nano Lett.* **2012**, *12*, 3483-3490.

[4] D. P. Dubal, D. S. Dhawale, R. R. Salunkhe, V. J. Fulari, C. D. Lokhande, *J. Alloys Compd.* **2010**, *497*, 166-170.

[5] a) D. P. Dubal, D. S. Dhawale, R. R. Salunkhe, S. M. Pawar, C. D. Lokhande, *Appl. Surf. Sci.* **2010**, *256*, 4411-4416; b) H. Y. Xu, S. Le Xu, X. D. Li, H. Wang, H. Yan, *Appl. Surf. Sci.* **2006**, *252*, 4091-4096.

[6] L. Zhang, Q. Zhou, Z. Liu, X. Hou, Y. Li, Y. Lv, *Chem. Mater.* **2009**, *21*, 5066-5071.

[7] H. W. Kim, Y. J. Kwon, H. G. Na, H. Y. Cho, C. Lee, J. H. Jung, *Microelectron. Eng.* **2015**, *139*, 60-69.

[8] a) H. Van Bui, F. Grillo, J. R. van Ommen, *Chem. Commun.* **2017**, *53*, 45-71; b) S. M. George, *Chem. Rev.* **2010**, *110*, 111-131; c) H. Pedersen, S. D. Elliott, *Theor. Chem. Acc.* **2014**, *133*, 1476; d) J. S. Price, P. Chadha, D. J. H. Emslie, *Organometallics* **2016**, *35*, 168-180.

[9] a) S. Mishra, S. Daniele, *Chem. Rev.* **2015**, *115*, 8379-8448; b) C. E. Knapp, C. J. Carmalt, *Chem. Soc. Rev.* **2016**, *45*, 1036-1064.

[10] a) A. Devi, *Coord. Chem. Rev.* **2013**, *257*, 3332-3384; b) P. Marchand, C. J. Carmalt, *Coord. Chem. Rev.* **2013**, *257*, 3202-3221; c) L. McElwee-White, *Dalton Trans.* **2006**, 5327-5333.

[11] a) T. Nakamura, *Phys. Status Solidi C* **2015**, *12*, 958-963; b) T. Nakamura, R. Tai, T. Nishimura, K. Tachibana, *J. Electrochem. Soc.* **2005**, *152*, C584-C587; c) S. Dhar, A. Varade, S. A. Shivashankar, *Bull. Mater. Sci.* **2011**, *34*, 11-18; d) S. I. Troyanov, O. Y. Gorbenko, A. A. Bosak, *Polyhedron* **1999**, *18*, 3505-3509; e) S. Kang, G. Brewer, K. R. Sapkota, I. L. Pegg, J. Philip, *IEEE Trans. Nanotechnol.* **2012**, *11*, 437-440.

[12] Z. Lipani, M. R. Catalano, P. Rossi, P. Paoli, G. Malandrino, *Chem. Vap. Deposition* **2013**, *19*, 22-28.

[13] A. R. Merritt, R. Rajagopalan, J. D. Carter, *Thin Solid Films* **2014**, *556*, 28-34.

[14] a) D. Barreca, E. Fois, A. Gasparotto, R. Seraglia, E. Tondello, G. Tabacchi, *Chem. Eur. J.* **2011**, *17*, 10864-10870; b) E. Fois, G. Tabacchi, D. Barreca, A. Gasparotto, E. Tondello, *Angew. Chem. Int. Ed.* **2010**, *49*, 1944-1948; c) G. Bandoli, D. Barreca, A. Gasparotto, R. Seraglia, E. Tondello, A. Devi, R. A. Fischer, M. Winter, E. Fois, A. Gamba, G. Tabacchi, *Phys. Chem. Chem. Phys.* **2009**, *11*, 5998-6007.

[15] G. Bandoli, D. Barreca, A. Gasparotto, C. Maccato, R. Seraglia, E. Tondello, A. Devi, R. A. Fischer, M. Winter, *Inorg. Chem.* **2009**, *48*, 82-89.
[16] a) D. Barreca, G. Carraro, A. Devi, E. Fois, A. Gasparotto, R. Seraglia, C. Maccato, C. Sada, G. Tabacchi, E. Tondello, A. Venzo, M. Winter, *Dalton Trans.* **2012**, *41*, 149-155; b) D. Barreca, G. Carraro, A. Gasparotto, C. Maccato, R. Seraglia, G. Tabacchi, *Inorg. Chim. Acta* **2012**, *380*, 161-166; c) G. Tabacchi, E. Fois, D. Barreca, G. Carraro, A. Gasparotto, C. Maccato, Modeling The First Activation Stages of the Fe(hfa)2TMEDA CVD Precursor on a Heated Growth Surface, in *Advanced Processing and Manufacturing Technologies for Nanostructured and Multifunctional Materials II*, John Wiley & Sons, Inc., **2015**, 83-90.
[17] G. Tabacchi, E. Fois, D. Barreca, A. Gasparotto, *Phys. Status Solidi A* **2014**, *211*, 251-259.
[18] G. Malandrino, R. G. Toro, M. R. Catalano, M. E. Fragalà, P. Rossi, P. Paoli, *Eur. J. Inorg. Chem.* **2012**, *2012*, 1021-1024.
[19] F. A. Cotton, R. H. Holm, *J. Am. Chem. Soc.* **1960**, *82*, 2979-2983.
[20] Y. Tohru, T. Toshihiro, R. Oliver, M. Teruaki, *Bull. Chem. Soc. Jpn.* **1991**, *64*, 2109-2117.
[21] A. Lopez-Periago, O. Vallcorba, C. Frontera, C. Domingo, J. A. Ayllon, *Dalton Trans.* **2015**, *44*, 7548-7553.
[22] N. A. Bailey, D. E. Fenton, M. V. Franklin, M. Hall, *J. Chem. Soc., Dalton Trans.* **1980**, 984-990.
[23] W. B. S. McCormack, C.A., *UK Patent GB 2022088A,* **1979**.
[24] G. Tabacchi, E. Fois, D. Barreca, A. Gasparotto, *Int. J. Quantum Chem.* **2014**, *114*, 1-7.
[25] B. S. Lim, A. Rahtu, J.-S. Park, R. G. Gordon, *Inorg. Chem.* **2003**, *42*, 7951-7958.
[26] L.-Y. Wang, X.-Q. Wang, K. Jiang, J.-L. Chang, Y.-F. Wang, *J. Mol. Struct.* **2007**, *840*, 14-21.
[27] F. H. Allen, *Acta Cryst.* **2002**, *B58*, 380-388.
[28] H. Wang, Z. Liu, C. Liu, D. Zhang, Z. Lü, H. Geng, Z. Shuai, D. Zhu, *Inorg. Chem.* **2004**, *43*, 4091-4098.
[29] D. Luneau, C. Stroh, J. Cano, R. Ziessel, *Inorg. Chem.* **2005**, *44*, 633-637.
[30] J. Ni, H. Yan, A. Wang, Y. Yang, C. L. Stern, A. W. Metz, S. Jin, L. Wang, T. J. Marks, J. R. Ireland, C. R. Kannewurf, *J. Am. Chem. Soc.* **2005**, *127*, 5613-5624.
[31] M. Cossi, V. Barone, B. Mennucci, J. Tomasi, *Chem. Phys. Lett.* **1998**, *286*, 253-260.
[32] L. Wang, Y. Yang, J. Ni, C. L. Stern, T. J. Marks, *Chem. Mater.* **2005**, *17*, 5697-5704.
[33] Pattern N° 024-0734, JCPDS (2000).
[34] B. D. Viezbicke, S. Patel, B. E. Davis, D. P. Birnie, *Phys. Status Solidi B* **2015**, *252*, 1700-1710.
[35] CrysAlisPro Software System, version 1.171.36.20; Agilent Technologies UK Ltd.: Oxford, U.K., 2012
[36] G. Sheldrick, *Acta Cryst.* **2008**, *A64*, 112-122.
[37] J. P. Perdew, K. Burke, M. Ernzerhof, *Phys. Rev. Lett.* **1996**, *77*, 3865-3868.
[38] a) H. Iikura, T. Tsuneda, T. Yanai, K. Hirao, *J. Chem. Phys.* **2001**, *115*, 3540-3544; b) A. W. Lange, M. A. Rohrdanz, J. M. Herbert, *J. Phys. Chem. B* **2008**, *112*, 6304-6308; c) J.-W. Song, T. Hirosawa, T. Tsuneda, K. Hirao, *J. Chem. Phys.* **2007**, *126*, 154105.
[39] M. J. Frisch, G. W. Trucks, H. B. Schlegel, G. E. Scuseria, M. A. Robb, J. R. Cheeseman, J. A. Montgomery Jr., T. Vreven, K. N. Kudin, J. C. Burant, J. M. Millam, S. S. Iyengar, J. Tomasi, V. Barone, B. Mennucci, M. Cossi, G. Scalmani, N. Rega, G. A. Petersson, H. Nakatsuji, M. Hada, M. Ehara, K. Toyota, R. Fukuda, J. Hasegawa, M. Ishida, T. Nakajima, Y. Honda, N. O. Kitao, H., M. Klene, X. Li, J. E. Knox, H. P. Hratchian, J. B. Cross, V. Bakken, C. Adamo, J. Jaramillo, R. Gomperts, R. E. Stratmann, O. Yazyev, A. J. Austin, R. Cammi, C. Pomelli, J. Ochterski, P. Y. Ayala, K. Morokuma, G. A. Voth, P. Salvador, J. J. Dannenberg, V. G. Zakrzewski, S. Dapprich, A. D. Daniels, M. C. Strain, O. Farkas, D. K. Malick, A. D. Rabuck, K. Raghavachari, J. B. Foresman, J. V. Ortiz, Q. Cui, A. G. Baboul, S. Clifford, J. Cioslowski, B. B. Stefanov, G. Liu, A. Liashenko, P. Piskorz, I. Komaromi, R. L. Martin, D. J. Fox, T. Keith, M. A. Al-Laham, C. Y. Peng, A. Nanayakkara, M. Challacombe, P. M. W. Gill, B. G. Johnson, W. Chen, M. W. Wong, G. C., J. A. Pople, *GAUSSIAN 09 (Revision D.02), Gaussian, Inc., Wallingford, CT,* **2009**.
[40] A. Bergner, M. Dolg, W. Küchle, H. Stoll, H. Preuß, *Mol. Phys.* **1993**, *80*, 1431-1441.
[41] T. H. Dunning Jr., P. J. Hay, in *Modern Theoretical Chemistry*, Plenum, New York, **1976**, Vol. 2, Chap. 1.
[42] a) L. Goodman, R. R. Sauers, *J. Comput. Chem.* **2007**, *28*, 269-275; b) A. E. Reed, L. A. Curtiss, F. Weinhold, *Chem. Rev.* **1988**, *88*, 899-926; c) E. D. Glendening, J. K. Badenhoop, A. E. Reed, J. E. Carpenter, J. A. Bohmann, C. M. Morales, F. Weinhold, in *NBO 5.0, Theoretical Chemistry Institute, University of Wisconsin, Madison, USA*, **2001**.

Chem. Eur. J. **2017**, *23*, 17954-17963, https://doi.org/10.1002/chem.201703423

Entry for the Table of Contents

FULL PAPER

A convenient route for the obtainment of Mn(II) diamine diketonate complexes is proposed. For the first time, the target adducts are characterized in detail by a combined experimental-theoretical approach. The compounds possess a monomeric structure, very favorable mass transport properties and clean fragmentation, all of which make them promising precursors for the vapor phase fabrication of manganese oxide nanosystems.

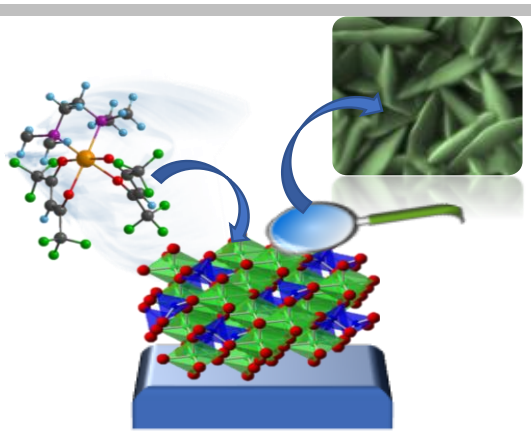

Prof. Chiara Maccato, Dr. Lorenzo Bigiani, Dr. Giorgio Carraro, Prof. Alberto Gasparotto, Dr. Roberta Seraglia, Dr. Jiyeon Kim, Prof. Anjana Devi, Prof. Gloria Tabacchi, Prof. Ettore Fois, Dr. Giuseppe Pace, Prof. Vito Di Noto, and Dr. Davide Barreca

Molecular engineering of Mn(II) diamine diketonate precursors for the vapor deposition of manganese oxide nanostructures